Journal of Alloys and Compounds 509 (2011) 5219–5229

Contents lists available at ScienceDirect

Journal of Alloys and Compounds

journal homepage: www.elsevier.com/locate/jallcom

First-principles calculations of elemental crystalline boron phases under high pressure: Orthorhombic B_{28} and tetragonal B_{48}

Sezgin Aydin, Mehmet Simsek*

Department of Physics, Faculty of Arts and Sciences, Gazi University, 06500 Teknikokullar, Ankara, Turkey

ARTICLE INFO

Article history:
Received 7 September 2010
Received in revised form 12 January 2011
Accepted 15 February 2011
Available online 22 February 2011

Keywords:
Crystal binding and equation of state
Elasticity
Electronic properties
Phase transitions
Computer simulations
High-pressure

ABSTRACT

The structural, electronic, mechanical properties and hardness of orthorhombic B_{28} and tetragonal B_{48} boron phases have been studied by first-principles of pseudopotential calculations. The results indicated that both boron phases are energetically and also mechanically stable. In addition to electronic properties of highly directional covalent bonds, mechanical properties, and also the Debye temperatures of structures support that both are superhard materials. Calculated electronic band structures and density of states revealed that orthorhombic B_{28} crystal is a semiconductor, and the tetragonal B_{48} is metallic. The pressure-dependent behaviors of both structures are different, and both are ultra-incompressible and anisotropic materials. The physical parameters of the structures such as lattice parameters, bond lengths, and also energy gaps between valance and conduction bands are closely sensitive to applied external pressures. By means of pressure–volume graphs, obtained EOSs for α-rhombohedral B_{12}, orthorhombic B_{28} and tetragonal B_{48} boron phases are compared with available data. However, energetically possible pressure-induced phase transitions among the purposed structures are predicted on the pressure range of 0–460 GPa. Furthermore, our calculations showed that for the pressures from 0 GPa to 24 GPa energetically the more stable elemental boron phase is α-rhombohedral B_{12}, and from 24 GPa to 106 GPa is orthorhombic B_{28}, and from 106 GPa to 460 GPa is α-Ga-type boron.

1. Introduction

Although many interesting properties have been investigated of elemental boron phases and its compounds, boron is an arguable element in the periodic table [1]. New findings on physical properties of boron and its compounds such as hardness, superconductivity, neutron shielding, and thermoelectricity have also been attractive to material research and for application [2]. However, boron has three valance electrons in four available orbitals, and most of its compounds have covalent and complex multicenter type bonds rather than ionic and/or metallic bonds [2–5]. Both these types of bonding together occur in electron deficient compounds [5]. Generally, there are quasi molecular basic units of building blocks in abundant compounds [3–7] such as icosahedron, hexagonal and pentagonal pyramids, octahedron and cubo-octahedron, in which the most common is icosahedron of B_{12}. In addition to building blocks, some of the elemental boron phases involve dopant atoms and/or molecules, which are located inter-icosahedra in three-dimensional network [7–13]. The different crystallization forms of elemental boron originate from the different linkings of the icosahedra and/or other units. It is well known that the simplest elemental solid phase of boron is α-rhombohedral B_{12} (α-boron, we shall indicate hereafter as α-r-B_{12}) and its structural, mechanical and other properties are intensively studied both experimentally [14–16] and theoretically [5,17–21] but some of the phases such as orthorhombic B_{28} (α-o-B_{28}) [22–27], tetragonal B_{48} (α-t-B_{48}) [28,29], and B_{50} (α-t-B_{50}) [31–34] structures are not fully understood yet. The other energetically favorable elemental boron phases [19], such as β-boron and tetragonal boron, exhibit strong deformation of icosahedra under high pressures and high temperatures (not under normal conditions), and two different high pressure boron phases, α-Ga-type and β-Ga-type boron structures, have semiconductor character [34,35]. However, more than a half hundred years ago, α-t-B_{50} crystal structure was introduced by Hoard et al. [31,32] and in that early study [31], they defined the structure as $B_{50} = B_{48}B_2$. Then, using the first-principles method, Li et al. [33] calculated electronic structures, total energies and optical properties of α-r-B_{12} and α-t-B_{50} crystal structures. Their results indicated that α-r-B_{12} is more stable than α-t-B_{50} at zero temperature [34]. Otherwise, using *ab-initio* calculations, the electronic properties, lattice dynamics, and electron-phonon coupling of α-Ga-type boron were studied by Ma et al. [36], and it is found that α-Ga boron is dynamically stable at high pressure.

On the other hand, many previous studies showed that increasing the pressure and/or temperature on the elemental boron phases always leads to the metallization [30,34,37,38]. We note here that,

* Corresponding author. Tel.: +90 312 202 12 35; fax: +90 312 212 22 79.
E-mail address: msimsek@gazi.edu.tr (M. Simsek).

0925-8388/$ – see front matter © 2011 Published by Elsevier B.V.
doi:10.1016/j.jallcom.2011.02.070

it was reported by Mailhiot et al. [30] and Eremets et al. [38], the phases of boron in icosahedral structure lose covalent bonding character to form a dense non-icosahedral structure. However, in the experiments to produce elemental Boron, while increasing the temperature (>1500 K) tetragonal and orthorhombic phases could be obtained, and also while increasing the pressure the phase transitions could also be enhanced [30,33–40]. A further increase in pressure dramatically decreases the resistance of compound, and then superconductivity would be accompanied by the loss of covalent bonding character [38]. It was also shown that many of polymorphic boron phases have unusual electronic structures at ambient conditions [39,40], and their mechanical and electronic properties were changed with the compressing. In this thought, Eremets et al. [38] found the phase transition from a nonmetal to a superconductor phase for β-boron at about 160 GPa, and the critical temperature of the transition increased from 6 K at 175 GPa to 11.2 K at 250 GPa. Haussermann et al. [34] pointed out a nonmetal–metal transition of elemental boron from α-r-B_{12} to α-Ga type phase at a pressure of about 74 GPa, and Mailhiot et al. [30] showed that the transition from the simplest boron phase (semiconductor) to a metallic body centered tetragonal structure is at approximately 210 GPa, and the transition to the face centered tetragonal structure occurs at approximately 360 GPa. It was shown [36] that the α-Ga-type boron was a good superconductor with strong anisotropy, resulting from the two-dimensional nature of the crystal structure, and also the calculated electron–phonon mass enhancement parameter was found to increase with pressure below 215 GPa.

On the other hand, in 1965, Wentorf [41] synthesized the "new" form of boron, but at that time, it was not decided whether the product was a new single crystalline phase or a mixture of new and known form of boron phases. More recently, different groups [22–26] synthesized the "new" superhard form of orthorhombic boron phase (γ-o-B_{28}) by using the experimental techniques as Wentorf's, and also they reported its structural, electronic and mechanical properties. It is noted that recent studies [24,25] showed that boron has been the second hardest elemental solid after diamond. Additionally, Jiang et al. [27] investigated the pressure dependent structural and mechanical properties up to 41 GPa of this phase by using first-principles. They [27] also found the ideal stress–strain behavior of orthorhombic B_{28} boron phase to better understand the phase stability and mechanical performance of this phase. However, a discussion about orthorhombic boron phase (γ-o-B_{28}) is continued by Zarechnaya et al. and Oganov et al., with more recent papers [22–26,42,43].

We note here that, in the more recent experimental study, Kurakevych and Solozhenko synthesized new boron subnitride phase ($B_{13}N_2$) and then, analyzed it by X-ray powder diffraction techniques [28,29]. In that study, the six phases were reported. They observed some narrower lines, overlapping with the lines of $B_{13}N_2$ for profile fitting of phase 2 and phase 4. They indicated in a mixture with β-boron (β-r-105), phase 4, an I-tetragonal boron-like phase and hBN, phase 3 and/or phase 6. Phase 2 was assigned for profile fitting as '$B_{50}N_2$' and they referred the early study of Ploog et al. [13]. In that early study, the boron-rich structures of tetragonal boron carbide composition $B_{48}B_2C_2$ (=$B_{50}C_2$) and boron nitride composition $B_{48}B_2N_2$ (=$B_{50}N_2$) were reported [13], and then Will and Kossobutzki [12] studied the boron rich structures, and in both studies the structures were assigned as in the space group P42m, not in P4n2 as in the text [28]. So, according to the cif code [29] of phase 2, which revealed a "new tetragonal phase", unfortunately it could be enshrouded by early compound of '$B_{50}N_2$' as was employed in the text [28,29]. Hereafter, we call it tetragonal B_{48} structure (α-t-B_{48}). Because tetragonal boron structure (α-t-B_{48}) consists entirely of icosahedra, any information obtained about it will be also helpful to understand the structures of other tetragonal phases such as B_{192}, B105, B_{50}, $B_{50}X_n$, etc.

In this study, we calculate physical properties such as structural parameters, electronic and mechanical properties of the novel synthesized orthorhombic boron phase (γ-o-B_{28}), and tetragonal B_{48} structure (α-t-B_{48}) by the first-principles calculations. To investigate the pressure-induced transitions, we optimized both phases under external hydrostatic pressure in the range of 0–460 GPa. We present an analysis of mechanical and electronic structure, charge transfer, and bonding properties of the constituent structures. For the sake of comparison of the properties of the structures and of the pressure-induced phase transitions, we also calculate mechanical and electronic properties of well-known α-boron, and also α-Ga type boron in given pressure range. Because of heavy computer cost, instead of all other phases our calculations are limited to add only two more stable phases.

2. Calculation details

In the present work, all calculations were performed by using CASTEP simulation package [44], based on the density functional theory. In the first stage of the calculations, all the atomic coordinates and unit cell parameters were fully relaxed for minimizing structures of Broyden, Fletcher, Goldfarb, Shanno (BFGS) scheme. The Vanderbilt ultrasoft pseudopotential [45] was used for modeling the ion–electron interactions. Exchange-correlation effects were treated within both the local density approximation (LDA) [46] and the generalized gradient approximation (GGA) [47] by the Perdew–Burke–Ernzerhof (PBE) [48] exchange correlation functional. The plane wave cut-off energy of 500 eV was employed. Brillouin zone integration was performed for k-point meshes generated by Monkhorst–Pack scheme, and they were chosen as $10 \times 10 \times 10$ for α-r-B_{12}, $10 \times 10 \times 8$ for γ-o-B_{28}, and $6 \times 6 \times 10$ for α-t-B_{48}. For the convergence, the ultra-fine setup of the software package was chosen, namely, it was assumed that all calculations were converged when the maximum ionic Hellman–Feynman force was below 0.01 eV/Å, maximum displacement between cycles was below 5.0×10^{-4} Å, maximum energy change was below 5.0×10^{-6} eV/atom, and maximum stress was below 0.02 GPa.

After optimization of the unit cells of the structures at ambient condition, volume-dependent relative energies ($\Delta E(V)$) of the α-r-B_{12}, γ-o-B_{28}, and α-t-B_{48} are plotted to determine the ground state phase of boron with LDA and GGA. Then, cohesive energy which is a key parameter to discuss energetic stability of the phases, $E_{form.}$=($E_{Total} - nE_{iso}/n$) is calculated (not include zero-point energy contribution), where E_{Total} is the total energy of the unit cell, E_{iso} is the energy of an isolated boron atom, obtained by placing boron atom into of sufficiently big box, n is the total number of atoms in the unit cell. Additionally, maximum uncertainty in calculated cohesive energies is 5.0×10^{-6} eV.

At the second stage of our calculation, the mechanical properties of the structures are examined. We determined the elastic constants by using stress–strain method. Then, physical properties such as bulk modulus, shear modulus, Young modulus and Poisson's ratios are calculated from following relations [49]:

(i) For hexagonal/rhombohedral crystals, there are five independent elastic constants; c_{11}, c_{33}, c_{44}, c_{12} and c_{13}. For these kinds of structures Reuss (R) and Voigt (V) bulk modulus and shear modulus are given as [49], $B_V = 1/9[2(c_{11} + c_{12}) + 4c_{13} + c_{33}]$, $G_V = 1/30[M + 12c_{44} + 12c_{66}]$, $B_R = C^2/M$ and $G_R = 5/2(C^2 c_{44} c_{66})/[3B_V c_{44} c_{66} + C^2(c_{44} + c_{66})]$, where the abbreviations are $C^2 = (c_{11} + c_{12})c_{33} - 2c_{13}^2$, $M = c_{11} + c_{12} + 2c_{33} - 4c_{13}$ and $c_{66} = (c_{11} - c_{12})/2$. Thus, the mechanical stability criteria are given as, $c_{44} > 0$, $c_{11} > |c_{12}|$, and $(c_{11} + 2c_{12})c_{33} > 2c_{13}^2$.

(ii) For tetragonal crystals, there are six independent elastic constants; c_{11}, c_{33}, c_{44}, c_{66}, c_{12} and c_{13}. Reuss and Voigt bulk modulus and shear modulus are given as [49], $B_V = 1/9[2(c_{11}+c_{12})+c_{33}+4c_{13}]$, $G_V = 1/30(M+3c_{11}-3c_{12}+12c_{44}+6c_{66})$, $B_R = C^2/M$, and $G_R = 15/\{(18B_V/C^2)+[6/(c_{11}-c_{12})]+(6/c_{44})+(3/c_{66})\}$, where M and C stand for $M = c_{11}+c_{12}+2c_{33}-4c_{13}$ and $c^2(c_{11}+c_{12})c_{33}-2c_{13}^2$.

Thus, the mechanical stability criteria are, $c_{11}>0$, $c_{33}>0$, $c_{44}>0$, $c_{66}>0$, $(c_{11}-c_{12})>0$, $(c_{11}+c_{33}-2c_{13})>0$, and $[2(c_{11}+c_{12})+c_{33}+4c_{13}]>0$.

(iii) For orthorhombic crystals, there are nine independent elastic constants, c_{11}, c_{22}, c_{33}, c_{44}, c_{55}, c_{66}, c_{12}, c_{13} and c_{23}. Reuss and Voigt bulk modulus and shear modulus are given as [49], $B_V = 1/9[c_{11}+c_{22}+c_{33}+2(c_{12}+c_{13}+c_{23})]$, $G_V = 1/15[c_{11}+c_{22}+c_{33}+3(c_{44}+c_{55}+c_{66})-(c_{12}+c_{13}+c_{23})]$, $B_R = \Delta/[c_{11}(c_{22}+c_{33}-2c_{23})+c_{22}(c_{33}-2c_{13}]-2c_{33}c_{12}+c_{12}(2c_{23}-c_{12})+c_{13}2c_{12}-c_{13}+c_{23}2c_{13}-c_{23}$, $G_R = 15/\{4[c_{11}(c_{22}+c_{33}+c_{23})+c_{22}(c_{33}+c_{13})+c_{33}c_{12}-c_{12}(c_{23}+c_{12})-c_{13}c_{12}+c_{13}-c_{23}c_{13}+c_{23}/\Delta+31/c_{44}+1/c_{55}+1/c_{66}$,

where $\Delta = c_{13}(c_{12}c_{23}-c_{13}c_{22})+c_{23}(c_{12}c_{13}-c_{23}c_{11})+c_{33}(c_{11}c_{22}-c_{12}^2)$. The mechanical stability criteria are, $c_{11}>0$, $c_{22}>0$, $c_{33}>0$, $c_{44}>0$, $c_{55}>0$, $c_{66}>0$, $[c_{11}+c_{22}+c_{33}+2(c_{12}+c_{13}+c_{23})]>0$, $(c_{11}+c_{22}-2c_{12})>0$, $(c_{11}+c_{33}-2c_{13})>0$, $(c_{22}+c_{33}-2c_{23})>0$.

Then, average bulk (B) and shear (G) modulus are defined as $B=(B_V+B_R)/2$ and $G=(G_V+G_R)/2$. Finally, Young modulus (E) and Poisson's ratio (ν) are calculated from the average bulk and shear modulus [50] as $E=(9GB)/(3B+G)$ and $\nu=(3B-E)/6G$, respectively.

Furthermore, using the parameters which are obtained from first-principles calculations into Gao's hardness method [51,52], the Vickers microhardness of the pure elemental boron structures is calculated. In this method, hardness of any μ-type bond in the structure is expressed by

$$H_V^{\mu} = \frac{350(N_e^{\mu})^{2/3}\exp(-1.19f_i^{\mu})}{(d^{\mu})^{2.5}}$$

where f_i^{μ}, d^{μ} and N_e^{μ} are ionicity, length and valance electron density of μ-type bond, respectively. f_i^{μ} is calculated by $f_i=[1-\exp(-|P_c-P|/P]^{0.735}$, where P is Mulliken population of the bond, P_c is the Mulliken population in the pure covalent solid of the same bond (it can be taken as 0.55 in the icosahedron-based boron structures [21]).

At the third step, to determine the possible phase transitions between all structures on the working pressure range (0–460 GPa), enthalpy functions, defined as $H=E+PV$, plotted as a function of pressure. Then, pressure-induced structural and electronic properties are calculated for the structures of α-r-B_{12}, γ-o-B_{28}, and α-t-B_{48}. Especially, to discuss whether the orthorhombic γ-o-B_{28} has ionic character, electronic charges on quasi-clustural units (icosahedron and B_2-dumbbell) and total charge of the unit cell are calculated.

In addition to these calculations, for the sake of comparison, calculated pressure–volume data are fitted to third order Birch–Murnaghan equation of state (EOS) [53],

$$P = \frac{3B_0}{2}\left[\left(\frac{V_0}{V}\right)^{7/3}-\left(\frac{V_0}{V}\right)^{5/3}\right]\left\{1+\frac{3}{4}(B_0'-4)\left[\left(\frac{V_0}{V}\right)^{2/3}-1\right]\right\},$$

to obtain bulk modulus and its first pressure derivative, which can give useful information about isotropy/anisotropy of the structures.

On the other hand, as the fundamental physical parameters, the Debye temperature [54] and also transversal and longitudinal sound velocities in the structures correlate many physical properties of solids [55], and the Debye temperature could be calculated from elastic constants [56] at low temperatures. According to the theory of Abrahams and Hsu [57], there is a relationship between Debye temperature and Vickers hardness of materials as $\theta_D \propto H^{1/2}\Omega^{1/6}M^{-1/2}$, where M is molar mass, Ω is molecular volume and H is Vickers hardness. However, there is another relationship between the Debye temperature and the average velocity of sound waves as [55,56], $\theta_D \propto \Omega^{-1/3}\nu_m$, where ν_m is the average velocity of sound waves.

3. Results

3.1. Pressure-induced lattice parameters, and bond structures

Calculated crystal structures and bond groups of optimized geometries of α-r-B_{12}, γ-o-B_{28}, and α-t-B_{48} phases at the ambient conditions are shown in Fig. 1(a)–(c), respectively. The space groups of unit cells of rhombohedral α-boron (α-r-B_{12}), the orthorhombic B_{28} (γ-o-B_{28}), and tetragonal B_{48} (α-t-B_{48}), are R-3m (166), Pnnm (58), and P-4n2 (118), respectively. There are some similarities and discrepancies between the purposed structures. Main similarity is that their building blocks are B_{12} icosahedra. Rhombohedral unit cell of the simplest elemental boron structure of α-r-B_{12} has one icosahedron with 12 boron atoms, which are located two kinds of non-equivalent sites (*polar* and *equatorial*), and linked to other icosahedra in the neighboring cells.

According to the bond lengths and their Mulliken population values, all bonds in the α-r-B_{12} can be classified into six different types (see Fig. 1(a)). B_p*–B_p* and Δ bonds are outside of icosahedra (inter-icosahedral bonds), others are inside (intra-icosahedral bonds). In unit cell, $3\times12=36$ valance electrons have construct 39 covalent bonds such as 9 inter- and 30 intra-icosahedral bonds. While B_p*–B_p* bonds link the polar atoms to the polar atoms of the neighboring icosahedra, multicenter Δ bonds link the equatorial atoms of three neighboring icosahedra to each other (sometimes, it is also named as weak three-center bond [39,40]). However, every boron atom in icosahedral unit is linked to the five-intra-icosahedral boron atoms. B_p–B_p bonds are between two polar atoms and are forming a B_p–B_p–B_p triangle in top and bottom of the icosahedra [21,39]. B_e–B_e bonds connect two neighboring B atoms at the equatorial sites. The remaining two types of bonds are formed between polar and equatorial B atoms. While B_p–B_e* bonds are forming a B_p–B_e–B_p triangle, B_p–B_e bonds are not forming a triangle [21]. On the other hand, orthorhombic unit cell of γ-o-B_{28} contains 28 boron atoms, with two icosahedra and two B_2 dumbbells which are located between icosahedra [24,33] (see Fig. 1(b)). In unit cell, $3\times28=74$ valance electrons have construct 92 covalent bonds (15 different types) such as 32 inter- and 60 intra-icosahedral bonds. It is noted that the 32 inter bonds that appear as 2 are between the atoms of B_2 dumbbells; and remaining bonds of the 20 are between icosahedra and dumbbells, and the 10 ones are between icosahedra. However, tetragonal unit cell of α-t-B_{48} consists of four icosahedra only, and has no extra boron atoms or chains between icosahedra (see Fig. 1(c)). Thus, there are $4\times12=48$ atoms in the unit cell. Furthermore, $3\times48=144$ valance electrons have construct 148 covalent bonds (13 different types) such as 28 inter- and 120 intra-icosahedral bonds.

The structural parameters and cohesive energies of α-r-B_{12}, γ-o-B_{28}, and α-t-B_{48} are calculated at ambient condition, and the results are tabulated in Table 1. As seen from Table 1, our calculated LDA and GGA values for all structures agree well with the previous results. Particularly, calculated structural parameters of α-t-B_{48} are in good agreement (~3%) with the experimental data of phase 2, which was assigned as '$B_{50}N_2$' in Ref. [28]. Both calculated cohesive energies are negative; −7.049 eV/atom for γ-o-B_{28}

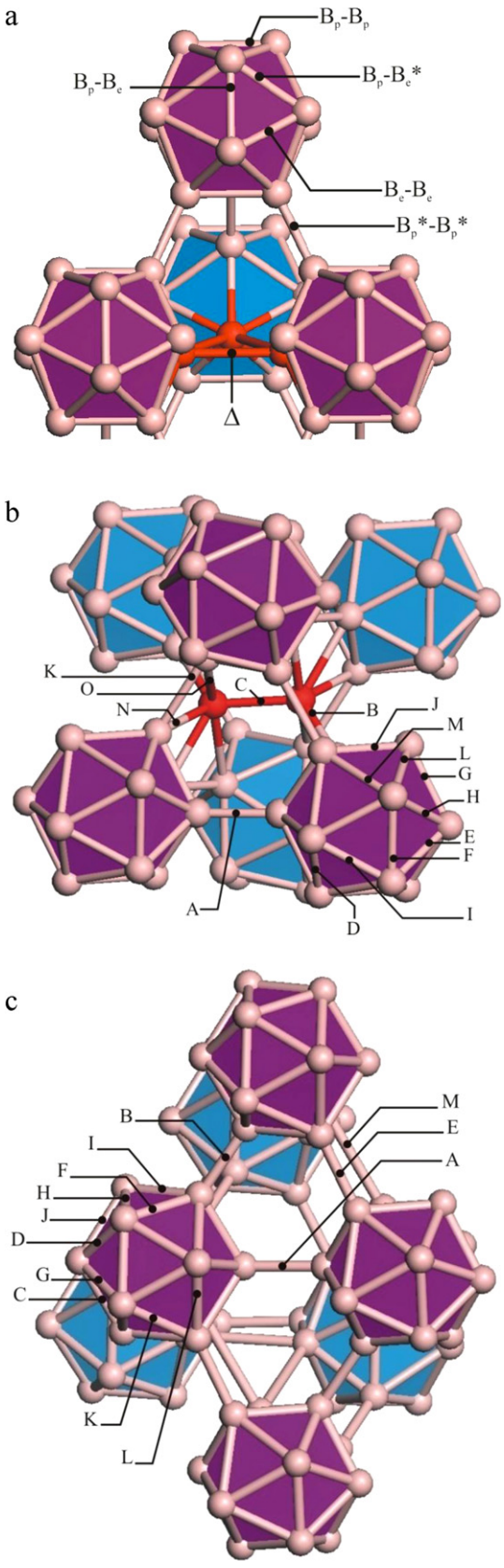

Fig. 1. Elemental crystal structures and bond groups (or types) in (a) α-boron α-r-B_{12}, (b) orthorhombic boron γ-o-B_{28}, (c) tetragonal boron α-t-B_{48}. For simplifying to see atomic locations and bonds, icosahedrons in front face were colored by purple and that of in back face were colored by blue. Pink spheres represent boron atoms and, atoms forming Δ-bond in α-r-B_{12} and B_2 dumbbell in γ-o-B_{28} are colored by red. (For interpretation of the references to color in this figure legend, the reader is referred to the web version of the article.)

Table 1
Calculated structural parameters and cohesive energies of three elemental boron phases with LDA and GGA approximations at 0 K and 0 GPa.

	α-r-B_{12}	γ-o-B_{28}	α-t-B_{48}
Crystal system	Rhombohedral	Orthorhombic	Tetragonal
Space group	R-3m (166)	Pnnm (58)	P-4n2 (118)
Atoms/unit cell	12	28	48
a (Å)	4.974 (GGA)	4.966 (GGA)	8.529 (GGA)
	4.969 (LDA)	4.965 (LDA)	8.488 (LDA)
	4.967[a]	5.054[c]	8.798[f]
	5.057[b]	5.058[d]	
		5.040[d]	
		5.056[e]	
		5.040[g]	
		5.054[h]	
b (Å)	–	5.535 (GGA)	8.529 (GGA)
		5.530 (LDA)	8.488 (LDA)
		5.620[c]	8.798[f]
		5.625[d]	
		5.610[d]	
		5.613[e]	
		5.610[g]	
		5.612[h]	
c (Å)	–	6.837 (GGA)	4.940 (GGA)
		6.801 (LDA)	4.937 (LDA)
		6.987[c]	5.037[f]
		6.988[d]	
		6.920[d]	
		6.971[e]	
		6.920[g]	
		6.966[h]	
α°	58.2 (GGA)	90	90
	58.1 (LDA)		
	58.7[a]		
	58.1[b]		
V_0 (Å^3)	83.452 (GGA)	187.927 (GGA)	359.326 (GGA)
	83.010 (LDA)	186.737 (LDA)	355.645 (LDA)
Cohesive energy (eV/atom)	−7.081 (GGA)	−7.049 (GGA)	−6.924 (GGA)
	−6.954 (LDA)	−6.930 (LDA)	−6.784 (LDA)

[a] Ref. [17].
[b] Ref. [15].
[c] Ref. [24].
[d] Ref. [25].
[e] Ref. [23].
[f] Ref. [28].
[g] Ref. [27].
[h] Ref. [57].

and −6.924 eV/atom for α-t-B_{48}, respectively. However, relative to that of simplest elemental boron structure (α-r-B_{12}), the cohesive energies are higher as +0.032 eV/atom and +0.157 eV/atom, respectively. So, according to the results of LDA and GGA, we can say that all three are energetically stable, and α-r-B_{12} is more stable than γ-o-B_{28} and α-t-B_{48}. As a result, the stability order from high to low is α-r-B_{12} > γ-o-B_{28} > α-t-B_{48} (see volume-dependent relative energies in Fig. 2(a)–(c)). As expected, calculated energies of unit lattices are lower within GGA than those within LDA. It would be noted here that van Setten et al. [58] recently reported that the β-boron (β-r-105) framework was +0.026 eV/atom higher in energy than α-r-B_{12} and also, according to their results the most stable structure was disordered 106 atom structure (β-r-106) at zero temperature, and taking the zero-point energy into account, the (β-r-106) unit cell boron wins at 4 meV with respect to α-r-B_{12} boron and becomes marginally more stable [24,58]. On the other hand, it was also found by Masago et al. [17] that α-boron (α-r-B_{12}) was more stable than β-boron (β-r-106), and according to their results [17] this did not change even if the zero-point energy and atomic disorders were considered.

The Mulliken population value of a bond can give useful information for characteristics of a bond (being as covalent or ionic) [21,40]. In the case if Mulliken population value is positive, and if it increases, i.e., covalency of the bond increases, then ionicity charac-

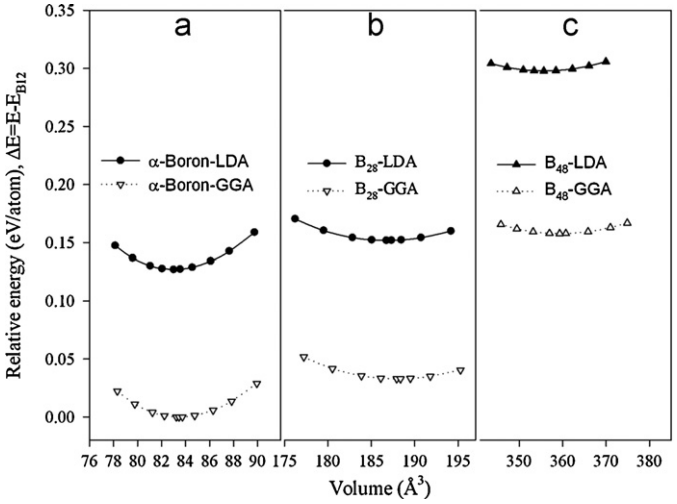

Fig. 2. Relative energy–volume curves for (a) α-r-B_{12}, (b) γ-o-B_{28}, (c) α-t-B_{48} with LDA and GGA. Non-equilibrium energies were obtained by applying isotropic expansion/contraction to equilibrium structure. The equilibrium energy value of α-r-B_{12} was chosen as the reference energy.

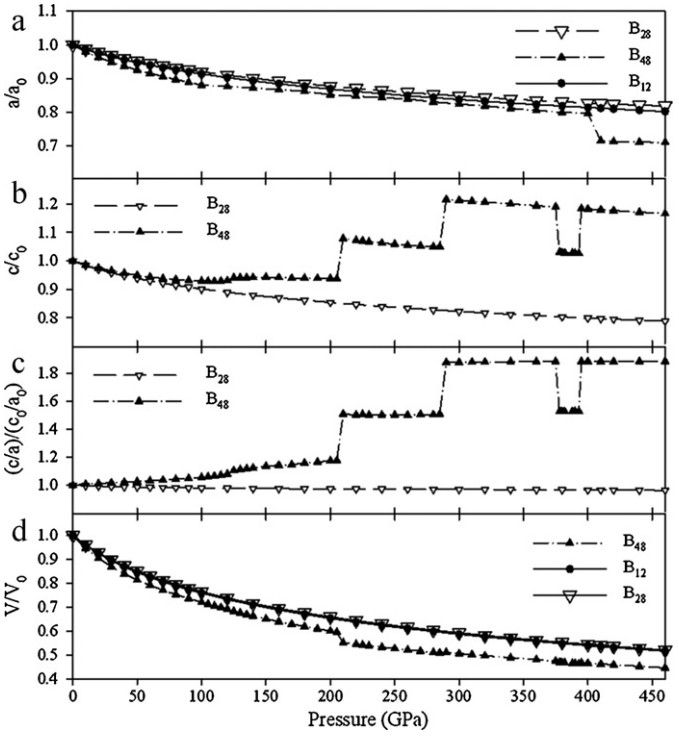

Fig. 4. Pressure dependence of the normalized lattice parameters and the unit cell volumes of α-r-B_{12}, γ-o-B_{28} and α-t-B_{48} elemental boron phases.

ter diminishes. It is well known that the covalent bond forms when atoms share electrons. Otherwise, if the value of Mulliken population is approaching to zero, ionicity character of bond becomes more dominant. Also, in order to characterize a bond as covalent or ionic, electron density maps can provide detailed information for certain bond directions. If electron density is located between two atoms, the covalent bond forms, and covalency of the bond increases as density increases. If electron density center is slip to each one of the atoms, the bond becomes ionic. Specially, the electron density maps for γ-o-B_{28} are given in Fig. 3(a)–(c). It is shown from these maps that boron atoms of B_2 dumbbells are strongly covalent bonded to each other (see Fig. 3(a)). When Mulliken population values of all bond groups in the structures with electron density maps given in Fig. 3(a)–(c) are considered, it is found that the inter-icosahedral bonds are strongly covalent.

It is also worth pointing out to investigate what happens on the lattice parameters and bond structures under the hydrostatic compression. As concerning structures, we are dealing with pressure dependence of the normalized lattice parameters of α-r-B_{12}, γ-o-B_{28} and α-t-B_{48}, as shown in Fig. 4(a)–(d). These figures revealed interesting results that directional bonding interactions between boron atoms, directed along the *c*-axis in γ-o-B_{28}, are leading to the least compressibility in the *c*-direction. On the other hand, for α-t-B_{48}, a/a_0, c/c_0 and V/V_0 curves have discontinuities in certain pressures (see Fig. 4(a)–(d)), and these discontinuities like a shape of steps and/or wells in lattice parameters of B_{48} structure is an interesting allocation from the other phases. As seen from Fig. 4(a) and (d), although prominent discontinuations of the value of lattice parameter a/a_0 and V/V_0 versus pressure plots only at 410 GPa and 215 GPa, respectively, at least five over range of induced pressure the lattice parameter c has discontinuities (see Fig. 4(b) and (c)). Generally, Fig. 4 says that all three structures are ultra-incompressible materials, the lattice parameters (*a* and *c*) and also volume of α-t-B_{48} are more compressible than those of α-r-B_{12} and γ-o-B_{28}. Otherwise, according to Fig. 4, γ-o-B_{28} is relatively incompressible material among them. However, in addition to discontinuities, pressure dependence of normalized *c/a* ratios showed contrary behavior in γ-o-B_{28} and α-t-B_{48} structures (see Fig. 4(c)). Thus, the sequences of high pressure structural discontinuities can be indicator for phase transitions and also changing of s–p hybridizations of the bands from s and p orbitals in the vicinity of the Fermi level.

The detailed effects of pressure-induced phase transitions and main discontinuities of the structural parameters, pressure dependence of the bond lengths and Mulliken populations for each bond group in the structures are calculated. It is shown that

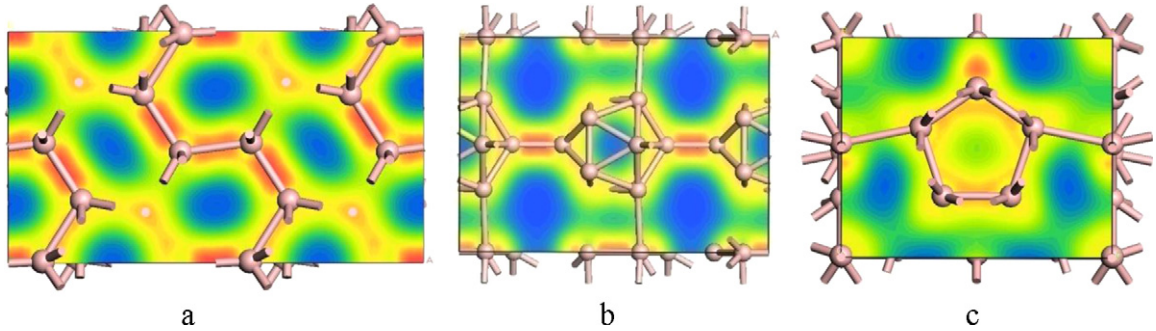

Fig. 3. Electron density maps for γ-o-B_{28}. (a) B_2 dumbbell and bonds linking it to icosahedrons in (0 0 1) plane. (b) Direct bonds between icosahedra in (0 2 0) plane. (c) The bonds of intra- and inter-icosahedron in (1 0 0) direction (as goes from blue to red, electron density increases). (For interpretation of the references to color in this figure legend, the reader is referred to the web version of the article.)

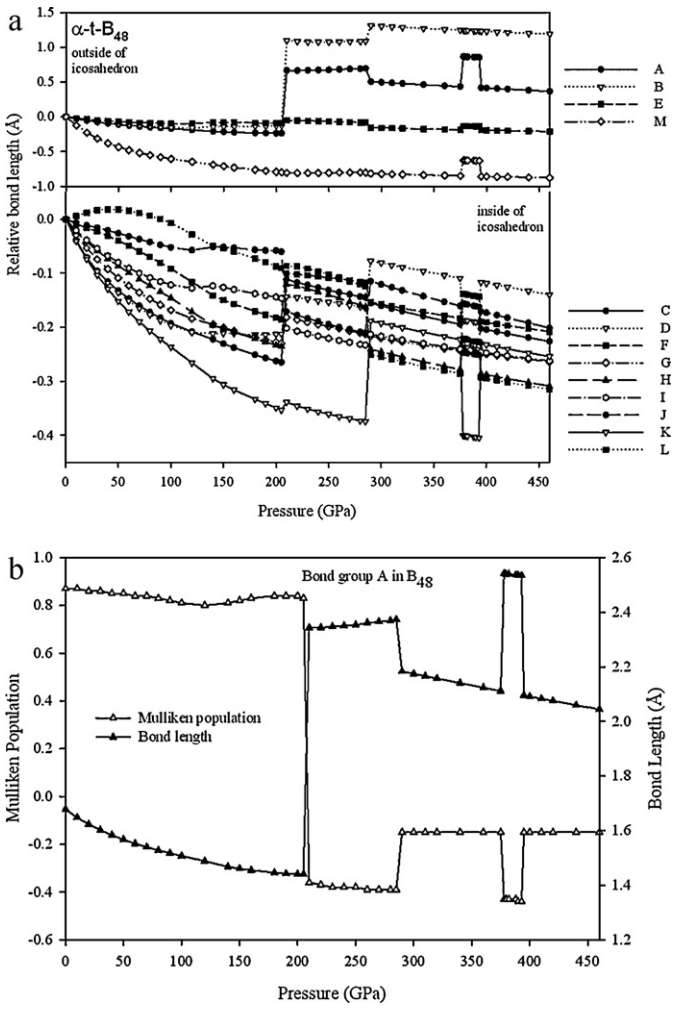

Fig. 5. Pressure dependence of the bond lengths for tetragonal α-t-B_{48}. Classifying of the bonds: (a) relative bond lengths, defined as lengthened (d–d_0) to the bond length (d_0) in 0 GPa for each bond and (b) pressure dependence of the Mulliken populations for the bond group A (inter-icosahedral bonds) in α-t-B_{48} as a function of pressure.

inter-icosahedral bonds ($B_p{}^*$–$B_p{}^*$ and Δ bonds [18,21,40]) exhibit more variation than intra-icosahedral bonds in α-r-B_{12}. If the bonds are ordered to the bond lengths, we obtain the sequence from high to low that $B_p{}^*$–$B_p{}^*$ > Δ > B_e–B_e > B_p–B_e > B_p–B_p > B_p–$B_e{}^*$. Other words, vacancies in the structure decrease rapidly, and equatorial region of the icosahedron contracts faster than polar region under pressure. Thus, our calculations showed that distinct topology of the icosahedron is conserved, and its existence in the structure remains under high pressures also. The possible explanations of this property are consistent with the results of the Refs. [19,59]. Generally, pressure-induced behavior of all bonds in γ-o-B_{28} similar to that of α-r-B_{12}, and bond group O is more affected than the others. Because of interesting behavior of pressure-induced parameters of α-t-B_{48}, the bond lengths and corresponding Mulliken populations of a special bond group (A) are presented in Fig. 5(a) and (b), respectively. It is seen from Fig. 5(a), pressure-induced behavior of the bonds of α-t-B_{48} are completely different from than that of both γ-o-B_{28} and α-r-B_{12}. There are discontinuous on pressure-depended relative bond lengths and also two main discontinuous in the enthalpy curve, will be discussed in next subsection. The pressure-depended discontinuities of bond lengths may affect the mechanical and electronic structure of α-t-B_{48}. As seen in Fig. 5(a), in the range of the 205–210 GPa (first break in the enthalpy curve), K, L and M bond groups are not significantly affected, but bond groups of A and B are controversy impressed and their bond lengths extensively grow up when the pressure increases from 1.441 Å to 2.343 Å and from 1.556 Å to 2.783 Å, respectively. These lengths of inter-icosahedral bonds are unexpected behaviors, and remaining bond groups are affected in medium scale. Interestingly, while the lengths of the bond groups (C, D, E, F, G and H) increase, those of bond groups I and J decrease. On the other hand, in the range of 285–290 GPa (the range of second discontinuity in the enthalpy curve), bond groups I and M are not affected from this discontinuity. While lengths of the bond groups (D, J and K) increase, that of the remaining bond groups decreases. So, α-t-B_{48} structure exhibits strong deformations under high compression, and the variation of bond number and bond lengths in the structure, leading to the phase transitions. Furthermore, we do not observe any discontinuity in the bonds at the range of phase transition pressures, except for phase transitions in the range of 375–395 GPa pressure.

However, in addition to bond length analysis, it would be worth to investigate the pressure effects on the electronic bonding character (see Fig. 5). We calculated Mulliken populations of each bond groups in α-t-B_{48} and obtained interesting results. We observed that although Mulliken population is directly proportional to bond length for some of bonds (bond groups G, I and J) in the structure, it is inversely proportion to the bond length for some of the bonds (bond groups A, B, E, F, H, K and L), and is not a relation between Mulliken population and bond length for some of bonds (bond groups C, D and M). As an example of inverse proportion, Mulliken populations of only bond group of A are plotted with bond lengths as a function of pressure in Fig. 5(b). As seen from Fig. 5(b), because Mulliken bond population of the bond (group A) is positive at the range of "relatively low compressions" (up to about 205 GPa), it has remained a strong covalent character up to 205 GPa. At the range of 205–210 GPa pressure, while Mulliken population drops to negative value unexpectedly, bond length increases rapidly also, then, the interaction between two atoms is becoming anti-bonding character. As a result, with the application of an external pressure, Mulliken population of a bond can be affected from external pressure and the bond can change its electronic character.

3.2. Elastic and mechanical properties

In order to find the mechanical properties such as bulk modulus, shear modulus, Young's modulus and Poison's ratio, we calculate the set of single crystal elastic constants, and tabulate in Table 2. However, bulk modulus and its first pressure derivative obtained from third order equation of state (EOS) are also listed in Table 2. As seen from the Table 2, both values of averaging bulk modulus (B) and shear modulus (G) for γ-o-B_{28} are the highest, and the corresponding values for α-t-B_{48} are the lowest. The order of bulk modulus from high value to low is given B(γ-o-B_{28}) > B(α-r-B_{12}) > B(α-t-B_{48}). This order is also valid for shear modulus and Young modulus. Furthermore, Young's modulus (E) and Poisson's ratio (ν) show technologic properties [50] of the materials, such as stiffness and also deformation to volume changing. Our values have shown that the highest value of Young's modulus and lowest Poisson's ratio are of γ-o-B_{28}. However, the highest Poisson's ratio (0.25) is of α-t-B_{48}, and corresponds to the larger deformation to the volume changing and it may have highest anisotropy among them. As seen from Table 2, our GGA results and also EOS results agree well with the other theoretical results. Finally, we have checked elastic stability of the structures, and it is found that all structures satisfy all stability criteria. So, they are mechanically stable under ambient condition.

In γ-o-B_{28} structure, the shortest covalent bond is an inter-icosahedral bond (d = 1.637 Å) in which bond group A. When Gao's hardness method [51] is applied to the structure, its cal-

Table 2
Calculated single-crystal elastic constants (c_{ij}, in GPa), Voigt (B_V), Reuss (B_R) and average bulk (B) and shear modulus (G), Young modulus (E) and Poisson's ratios (ν), Vickers microhardness (H), zero pressure bulk modulus (B_0) and its pressure derivative (B_0') which obtained by fitting pressure-volume data to third order Birch–Murnaghan equation of state.

	α-r-B_{12}	γ-o-B_{28}	α-t-B_{48}
c_{11}	474	641; 609[f]	338
c_{22}	–	574; 543[f]	–
c_{33}	632	477; 456[f]	365
c_{44}	225	250; 241[f]	133
c_{55}	–	238; 224[f]	–
c_{66}	–	269; 254[f]	36
c_{12}	109	82; 84[f]	32
c_{13}	44	39; 42[f]	97
c_{23}	–	83; 85[f]	–
B_0 (GPa)	219.8	230.6	162.0
	218.4[a]	221.7[e1]	
	213–224[b]	227.0[e2]	
	249[c]; 266[c]	222[f]	
	185(7)[d]	237[g]	
B_0'	3.69	3.61	3.87
	4.8[a]	3.63[e1]	
	4.0[b]	2.22[e2]	
		3.67[f]	
		2.7[g]	
B_V	219.1	233.3	165.7
B_R	217.9	229.7	163.1
B (GPa)	218.5	231.5	164.4
		224[f]	
G_V	218.8	250.5	114.6
G_R	213.2	248.1	86.0
G (GPa)	216.0	249.3	100.3
		236[f]	
E (GPa)	487.4	550.3	250.0
		524[f]	
ν	0.13	0.10	0.25
		0.11[f]	
H (GPa)	39.5	42.1	40.0

[a] Ref. [17].
[b] Ref. [15].
[c] Ref. [16].
[d] Ref. [29].
[e] Ref. [25] (e1: 0 K, e2: 300 K).
[f] Ref. [27].
[g] Ref. [65].

culated valance electron density and individual bond hardness are 0.650 and 76.6 GPa, respectively, the results indicate that this bond is the hardest among all the bonds. The second hardest bond (H = 74.0 GPa) is also inter-icosahedra bond (d = 1.650 Å, with valance electron density of 0.635), which is forming between the icosahedral B atom and one of the B atoms of quasi-molecular B_2 dumbbells. Both of these values are highest among those of all constituent structures. Third order hardest bonds (d = 1.706 Å) are between B atoms of quasi-molecular B_2 dumbbells. It is interesting that the "soft" covalent bonds are in γ-o-B_{28} structure (d = 2.034 Å) which are between the icosahedral B atoms and one of the B atoms of quasi-molecular B_2 dumbbells. Corresponding valance electron density and individual bond hardness are 0.315 and 27.4 GPa, respectively. The hardest and third hardest bonds are in the same direction, both are parallel to each other, are also perpendicular to (1 0 0) surface, so this might increase the directional hardness of the structure. Then, by using Gao et al.'s hardness method [51], we calculated the Vickers microhardness of the γ-o-B_{28} as 42.1 GPa, which is higher than that of superhardness limit (40 GPa), but it is very much lower than that of the experimental results ($H \sim 50$ GPa) of Solozhenko et al. [22], and (H = 58 GPa) of Zarechnaya et al. [25].

On the other hand, inter-icosahedral bonds in α-t-B_{48} structure have strong covalent characters, the shortest ones have the bond length of 1.678 Å in all bonds of the structure. Corresponding valance electron density and individual bond hardness of these bonds are 0.511 and 61.3 GPa, respectively. Second hardest bonds are also another inter-icosahedral bonds (d = 1.687 Å) and corresponding valance electron density and individual bond hardness are 0.502 and 59.9 GPa, respectively. On the other hand, the weakest covalent bonds are also another inter-icosahedral bonds (d = 2.449 Å) and corresponding valance electron density and individual bond hardness are 0.141 and 10.1 GPa, respectively. These bonds are constructed by replacing the two-center strong covalent bonds with weak three-center long and soft bonds. These values are also lowest between all structures. Thus, in both structures the intermediate bonds are located intra-icosahedra of B_{12} (1.700 Å < d < 1.854 Å). It should be noted that the calculated Vickers microhardness of α-t-B_{48} is 40.0 GPa, and is lower than that of γ-o-B_{28} but slightly higher than that of α-r-B_{12} (see Table 2). However, we can classify it as a superhard material. We note here that it has been speculated that tetragonal borides ($B_{48}B_2C_2$, $B_{48}B_2N_2$) could have novel superhard properties [12,13].

3.3. Electronic structures

Calculated electronic band structures, and partial density of states (PDOSs) and total density of states (DOSs) for α-r-B_{12}, γ-o-B_{28} and α-t-B_{48} are shown in Fig. 6(a)–(c), respectively. It is to be noted that the calculated indirect band gaps of 1.661 eV for α-r-B_{12}, and 1.685 eV for γ-o-B_{28} are in good agreement with the result (1.427 eV) of Ref. [18], and (1.700 eV) of Ref. [25], respectively. PDOSs of optimized three structures together indicate that s–p hybridization becomes dominant at lower energy bands (see Fig. 6(a)–(c)). Generally, the contribution of s electrons to the filled states between the Fermi level (E_f) and ∼−8 eV is rather small, and p electrons become dominant with decreasing the energies of individual bands, so the s–p hybrid orbitals give rise to peaks on the lower energy scale. As seen from Fig. 6(a) and (b), upper valance bands of α-r-B_{12} and γ-o-B_{28} are just below the Fermi levels but the electronic band structure and PDOS of γ-o-B_{28} are different from those of α-r-B_{12}. However, in γ-o-B_{28} structure, PDOS of B_2 dumbbell becomes sharper near the Fermi level and upper energy levels are shifted to the Fermi level because of "dopant ion" effects of B_2 dumbbell. The nearly flat bands located just below the Fermi level, originated from 2p orbital, which have sharp peak very close to the Fermi level in DOS graph (see Fig. 6(b)). The calculated band structures and DOSs curves both revealed that all three have different electronic characters: α-r-B_{12} is a semiconductor, γ-o-B_{28} is an unusual semiconductor, and α-t-B_{48} is metallic. However, Fig. 7 shows that nonmetal–metal transition of α-r-B_{12} at 150 GPa, after this pressure, and then the energy gap between valance and conduction bands (E_{gap}) value goes to zero. In fact, this diminishing trend versus to pressure would be amelioration of metallization and conductivity, and also superconductivity in the structure. Zhao and Lu [59] and Shirai et al. [60] reported this value as 160 GPa in different times in the literature. Then, we can say that our metallization pressure (150 GPa) agrees well with those of Zhao and Lu [59] and Shirai et al. [60]. The first obvious difference between normal semiconductor and γ-o-B_{28} is that B_2 dumbbell behaves like "dopant ion" in boron-rich borides [24] (see partial density of states of B_2 in Fig. 6(b), it is different near the Fermi level as of semiconductor or metals). In the following we will call "dopant ion" as a quasi-cluster. The reason for this rapid diminish of E_{gap} around 415 GPa of γ-o-B_{28} can be explained as "metallization effect", and also phase transition (see Fig. 7). When the trend of the pressure-induced E_{gap} is considered, metallization in γ-o-B_{28} can be expected at pressure higher than 460 GPa, hence it would be predicted possible metallization pressure by extrapolation as 501.1 GPa.

On the other hand, as seen from Fig. 6(c), the location of Fermi level of α-t-B_{48} among the unoccupied bands, and none zero DOS at Fermi level are similar properties to that of the structure of β-105

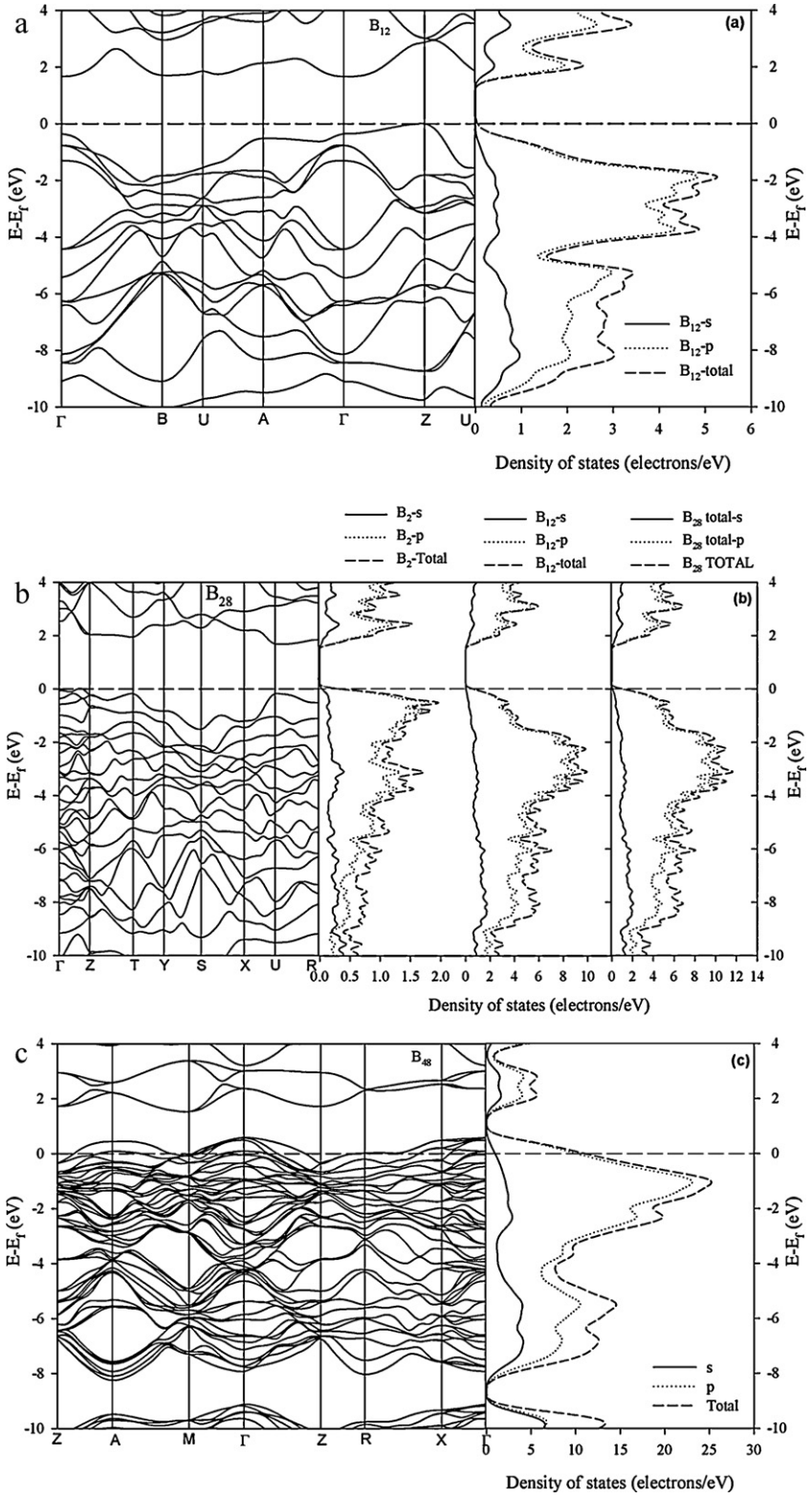

Fig. 6. Calculated electronic band structures, and partial and total density of states (DOSs) for (a) α-r-B_{12}, (b) γ-o-B_{28}, and (c) α-t-B_{48} elemental boron phases. Calculated Fermi energies for α-r-B_{12}, γ-o-B_{28}, and α-t-B_{48} are 8.169 eV, 9.225 eV and 5.685 eV, respectively, and they are automatically set to zero in the figures.

[19]. The high energy parts of occupied bands and also unoccupied π^* bands of p electrons appear explicitly vicinity of the Fermi level of α-t-B_{48}, originated predominantly from 2p states of B atoms. We can say that it is metallic and then, DOS value never goes to zero at Fermi level in the whole range of constituent external pressure (0–460 GPa). Generally, the metallic property of α-t-B_{48} can be attributed to the increasing of p-type states to bands higher than the Fermi level. This common behavior comes from of extraordinary inter-icosahedral bonds, and they caused distorted icosahedra and also strong deformations in crystal structure as indicated above.

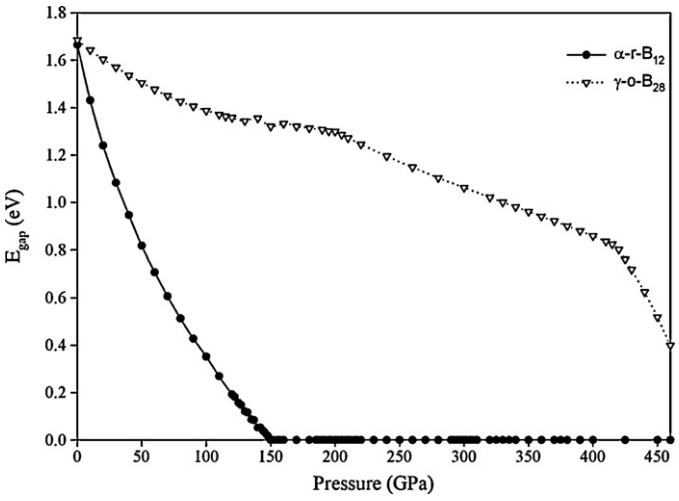

Fig. 7. Pressure-dependent energy gap curves for α-r-B_{12} and γ-o-B_{28} structures. We predict possible metallization pressure as 150 GPa for α-r-B_{12}, and (by extrapolation) as 501.1 GPa for γ-o-B_{28} structure.

3.4. Pressure-induced phase transitions

Recently, nonmetal–metal transitions in boron group elements and electronic relationships between icosahedral and metallic close-package modification for boron were studied previously [19,24,34,37,59]. Also, high pressure properties and phase diagrams of boron were studied by Shirai et al. [61] theoretically, and they discussed pressure-dependence of the properties, and it was reported that α-boron was the most stable phase at low temperatures and β-boron phase was most favorable phase at high temperatures [17,19,24,61]. On the other hand, using quasi-harmonic approximation [61,62], it was reported high pressure results of experiments and theoretic studies of α- and β-boron phases to understand of high pressure properties of icosahedrons-based boron phases.

Here, relative enthalpy-pressure curves for γ-o-B_{28} and α-t-B_{48} structures are plotted to determine possible phase transitions in Fig. 8 with together two other stable phases, α-r-B_{12} and α-Ga-type boron, which are generally known as low and high pressure phases of boron [17,24,27,34,35], respectively.

As seen from Fig. 8, there are crossing points of the enthalpy–pressure curves of constituent four stable boron structures. Our GGA calculations predict that the transition at 19.73 GPa

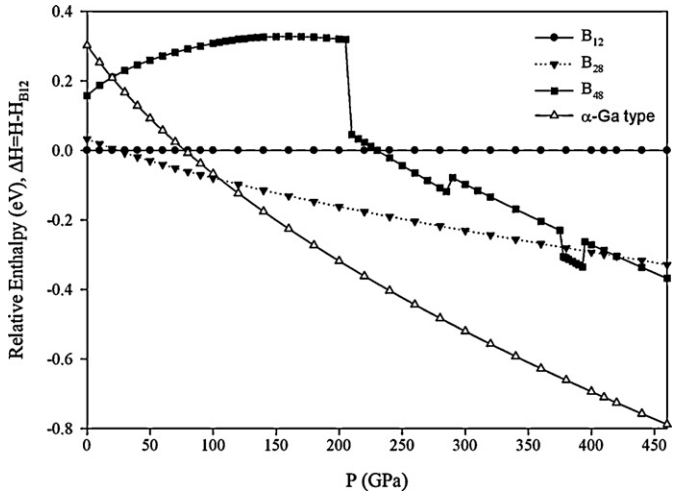

Fig. 8. Relative enthalpy–pressure curves for α-r-B_{12}, γ-o-B_{28}, α-t-B_{48} and α-Ga-type boron phases. Enthalpies are shown relative to α-r-B_{12} at constituent pressures.

pressure for α-t-B_{48} → α-Ga-type boron phase (metal to nonmetal), and the other transition as α-r-B_{12} → γ-o-B_{28} at 24.35 GPa, which is higher than the experimental results of Oganov et al. [24] (19 GPa), and Zarechnaya et al. [25] (20 GPa). It would be noted here that Ma et al. [63] presented R-105 boron transforms above 10 GPa at high temperature to a tetragonal phase that remains on P–T quenching, but less than 19 GPa, after heating at temperatures higher than 1500 K. Also, Oganov et al. [24] reported that different phase transitions were below 19 GPa (see Fig. 3 of Ref. [24]). According to our calculations (see Fig. 8), over this pressure (24.35 GPa), α-r-B_{12} is not a ground state of elemental boron. The transition from α-r-B_{12} to α-Ga-type boron is predicted at 77.48 GPa, and this value is higher than the results of previous studies, 74 GPa [34] and 71 GPa [35]. The transition γ-o-B_{28} → α-Ga-type boron occurs at 106.45 GPa and this value is higher than the experimental observations, reported as 89 GPa by Oganov et al. [24], and 88 GPa by Zarechnaya et al. [25].

Furthermore, applying pressure up to 460 GPa, α-Ga-type boron phase remains a low enthalpy structure, so it may be ground state of boron, but extra transitions occur between other metastable structures as follows: As seen from Fig. 8, after the first dropping (at the range of 205–210 GPa), the curve of α-t-B_{48} crosses the curve of α-r-B_{12} at 230 GPa, and then, as pressure increases, three times of phase transitions between α-t-B_{48} and γ-o-B_{28} structures are predicted at 376.80 GPa, 394.20 GPa, and 420 GPa, respectively, but their enthalpies are never lower than that of α-Ga-type boron phases up to the studied highest pressure (460 GPa).

In addition to the phase transitions, there are interesting discontinuities in the pressure-dependent enthalpy curve of α-t-B_{48}, except phase transitions, at the ranges of 205–210 GPa, 285–290 GPa, 375–380 GPa, and 393–395 GPa. Up to first discontinuity region (205–210 GPa), the enthalpy curve is growing up unexpectedly, this is contrary behavior to that of other three phases (see Fig. 8) but similar to the behavior of T-192 and β-106 phase diagrams of Oganov et al. [24] (see Fig. 3 of Ref. [24]). At this discontinuity, because of the structural changes (discussed above), the relative enthalpy of α-t-B_{48} sharply drops from 0.32 eV to 0.04 eV. Also, as seen from Figs. 4 and 5, crystal structure completely changes, i.e., the space group changes from P-4n2 to P42/nnm, and covalent bond numbers increases from 148 to 184. As a consequence of this compressing behavior, the volume of the unit cell shrinking from 213.82 $Å^3$ to 198.05 $Å^3$. Because of the pressure dependence of the bond lengths, distorted icosahedra occur, and their quasi-cluster units closure to each other. It is noted that this kind of similar interesting distortion behavior of β-106 boron phases at 205 GPa was reported by Siberchicot [19]. In the second discontinuity region (285–290 GPa), there are contrary behaviors such as space group does not change, and while covalent bond number of 184 decreases to 172, volume of 182.62 $Å^3$ increases to 183.37 $Å^3$, and also, relative enthalpy increases from −0.15 eV to −0.08 eV. At the third and fourth discontinuity regions, 375–380 GPa,and 393–395 GPa, respectively, there are two phase transitions between both structure. At the third region the transition is γ-o-B_{28} → α-t-B_{48} and at fourth is contrary transition as α-t-B_{48} → γ-o-B_{28}. Interestingly, enthalpy curve of α-t-B_{48} generally behaves as broken linear lines (with different slopes) from 210 GPa to 460 GPa. These are extremely interesting behavior of elemental boron phases.

3.5. Sound velocities and Debye temperatures

Finally, calculated sound velocities and Debye temperatures of α-r-B_{12}, γ-o-B_{28} and α-t-B_{48} are tabulated in Table 3. As shown in Table 3, the Debye temperature of α-r-B_{12} structure is higher than that of γ-o-B_{28} and α-t-B_{48}, but the sound velocity in the γ-o-B_{28} structure is higher than that of α-r-B_{12} and α-t-B_{48}. It is noted

Table 3
Calculated unit cell densities (in g/cm^3), transverse (v_t), longitudinal (v_l), and average (v_m), sound velocities (in m/s), and Debye temperature θ_D (in K) of three elemental boron phases.

Compound	ρ (g/cm^3)	v_t	v_l	v_m	θ_D
α-r-B_{12}	2.58	9148.01	14007.98	10026.51	1241 1430[a]
γ-o-B_{28}	2.68	9653.91	14519.78	10557.25	997
α-t-B_{48}	2.40	6467.35	11149.31	7177.01	546

[a] Ref. [17].

that the Debye temperature of α-r-B_{12} structure agrees well with previous calculation [17] (see Table 3). Thus, according to the theory of Abrahams and Hsu [57], and also conclusions of Hao et al. [64], our results indicate that γ-o-B_{28} should be harder than both α-r-B_{12} and α-t-B_{48} phases. This result is in good agreement with hardness order (explained previous subsection), H(γ-o-B_{28}) > H(α-r-B_{48}) > H(α-t-B_{12}). Furthermore, the density order of constituent structures from the high value to low is ρ(γ-o-B_{28}) > ρ(α-r-B_{12}) > ρ(α-t-B_{48}), and so, it is the same order with that of bulk modulus. However, orders of hardness and bulk modulus are not same. In other words, we can say that there is not a direct relation between hardness and bulk modulus in consequent structures. As a general point of view, when we consider effects of pressure and temperature on a given phase, density of unit cell can be used to discuss stability of the boron polymorphs. While dense phases are stable at high pressure and low temperature, dilute phases are stable at low pressure and high temperature [24,57,64]. According to this suggestion, stability order at high pressure should be γ-o-B_{28} > α-r-B_{12} > α-t-B_{48}, as independent of temperature.

4. Conclusions

We calculated the structural, electronic and mechanical properties of constituent phases of elemental boron crystal on pressure range of 0–460 GPa by using first-principles calculations of density functional theory. The cohesive energies show that α-r-B_{12}, γ-o-B_{28} and α-t-B_{48} are energetically stable, and also, all three structures satisfy the mechanical stability conditions. Obtained EOSs for three phases are compared to available data, which are consistent with the available experimental results. Calculated Vickers microhardness of α-t-B_{48} is 40.0 GPa, lower than that of γ-o-B_{28} (42.1 GPa), but slightly higher than that of α-r-B_{12} (39.5 GPa). However, all three can be classified as superhard materials, and our calculated hardness order coincides with hardness-Debye temperature relationship. The details pressure dependence of lattice parameters, bond lengths, Mulliken bond populations, energy gap and density of states are investigated. We observe icosahedron-based modifications, and, generally, the pressure-dependent behaviors of three structures are different, and also all three phases are ultra-incompressible and anisotropic materials. Electronic band structure and the pressure-dependent energy gap curves revealed that α-r-B_{12}, and γ-o-B_{28} are nonmetal and α-t-B_{48} is metal, but while increasing the pressure, nonmetal–metal transitions occur between α-r-B_{12}, γ-o-B_{28} and α-t-B_{48} boron phases.

Our calculations show that the pressure-dependent enthalpy curves have different shapes in constituent pressure range. The enthalpy curve of α-t-B_{48} behaves as broken linear lines (with different slopes) at the pressure from 210 GPa to 460 GPa. From our calculations and previous results, α-Ga-type boron phase may be the best candidate for the high pressure phase of boron. Finally, the pressure-dependent behaviors of constituent phases of elemental boron crystal are extremely interesting, and we hope that it would be worth to increase the technologic applicability of the elemental boron structures.

Acknowledgments

This work is supported partly by the State of Planning Organization of Turkey under Grant No. 2001K120590 and Gazi University BAP, under grant no. 05/2010-82. We are grateful to anonymous referees for useful comments and suggestions.

References

[1] B.E. Douglas, S.-M. Ho, Structure and Chemistry of Crystalline Solids, Springer, New York, 2006.
[2] B. Albert, H. Hillebrecht, Angew. Chem. Int. Ed. 48 (2009) 8640.
[3] M. Fujimori, T. Nakata, T. Nakayama, E. Nishibori, K. Kimura, M. Takata, M. Sakata, Phys. Rev. Lett. 82 (1999) 4452.
[4] J. He, E. Wu, H. Wang, R. Liu, Y.J. Tian, Phys. Rev. Lett. 94 (2005) 015504.
[5] K. Shirai, Phys. Rev. B 55 (1997) 12235.
[6] G. Ning, R.L. Flemming, J. Appl. Crystallogr. 38 (2005) 757.
[7] A. Zalkin, D.H. Templeton, J. Chem. Phys. 18 (1950) 391.
[8] G. Will, K.H. Kossobutzki, J. Less-Common Met. 47 (1976) 43.
[9] H. Gou, J. Zhang, F. Gao, J. Phys.: Condens. Matter 20 (2008) 505211.
[10] J.P. Mercurio, J. Etourneau, R. Naslain, P. Hagenmuller, J. Less-Common Met. 47 (1976) 175.
[11] R. Naslain, A. Guette, P. Hagenmuller, J. Less-Common Met. 47 (1976) 1.
[12] G. Will, K.H. Kossobutzki, J. Less-Common Met. 47 (1976) 33.
[13] K. Ploog, H. Schmidt, E. Amberger, G. Will, K.H. Kossobutzki, J. Less-Common Met. 29 (1972) 161.
[14] G. Will, B. Kiefer, Z. Anorg, Z. Anorg. Allg. Chem. 627 (2001) 2100.
[15] B.F. Decker, J.S. Kasper, Acta Crystallogr. 12 (1959) 503.
[16] R.J. Nelmes, J.S. Loveday, D.R. Allan, J.M. Besson, G. Hamel, P. Grima, S. Hull, Phys. Rev. B 47 (1993) 7668.
[17] A. Masago, K. Shirai, H. Katayama-Yoshida, Phys. Rev. B 73 (2006) 104102.
[18] S. Lee, D.M. Bylander, L. Kleinman, Phys. Rev. B 45 (1992) 3245.
[19] B. Siberchicot, Phys. Rev. B 79 (2009) 224101.
[20] N. Vast, S. Baroni, G. Zerah, J.M. Besson, A. Polian, M. Grimsditch, J.C. Chervin, Phys. Rev. Lett. 78 (1997) 693.
[21] X. Guo, J. He, Z. Liu, Y. Tian, J. Sun, H.T. Wang, Phys. Rev. B 73 (2006) 104115.
[22] V.L. Solozhenko, O.O. Kurakevych, A.R. Oganov, J. Superhard Mater. 30 (2008) 428.
[23] E.Y. Zarechnaya, L. Dubrovinsky, N. Dubrovinskaia, N. Miyajima, Y. Filinchuk, D. Chernyshov, V. Dmitriev, Sci. Technol. Adv. Mater. 9 (2008) 044209.
[24] A.R. Oganov, J. Chen, C. Gatti, Y. Ma, Y. Ma, C.W. Glass, Z. Liu, T. Yu, O.O. Kurakevych, V.L. Solozhenko, Nature 457 (2009) 863.
[25] E.Y. Zarechnaya, L. Dubrovinsky, N. Dubrovinskaia, Y. Filinchuk, D. Chernyshov, V. Dmitriev, N. Miyajima, A. El Goresy, H.F. Braun, S. Van Smaalen, I. Kantor, A. Kantor, V. Prakapenka, M. Hanfland, A.S. Mikhaylushkin, I.A. Abrikosov, S.I. Simak, Phys. Rev. Lett. 102 (2009) 185501.
[26] See EPAPS Document No. E-PRLTAO-102-018921 for additional information on http://www.aip.org/pubservs/epaps.html.
[27] C. Jiang, Z. Lin, J. Zhang, Y. Zhao, Appl. Phys. Lett. 94 (2009) 191906.
[28] O.O. Kurakevych, V.L. Solozhenko, Acta Crystallogr. C 63 (2007) i80.
[29] Supplementary data for the paper [28] are from IUCr electronic archives. (Reference: SQ3084).
[30] C. Mailhiot, J.B. Grant, A.K. McMahan, Phys. Rev. B 42 (1990) 9033.
[31] J.L. Hoard, S. Geller, R.E. Hughes, J. Am. Chem. Soc. 73 (1951) 1892.
[32] J.L. Hoard, R.E. Hughes, D.E. Sans, J. Am. Chem. Soc. 80 (1958) 4507.
[33] D. Li, Y.-N. Xu, W.Y. Ching, Phys. Rev. B 45 (1992) 5895.
[34] U. Haussermann, S.I. Simak, R. Ahuja, B. Johansson, Phys. Rev. Lett. 90 (2003) 065701.
[35] D.E. Segall, T.A. Arias, Phys. Rev. B 67 (2003) 064105.
[36] Y. Ma, J.S. Tse, D.D. Klug, R. Ahuja, Phys. Rev. B 70 (2004) 214107.
[37] D.N. Sanz, P. Loubeyre, M. Mezouar, Phys. Rev. Lett. 89 (2002) 245501.
[38] M.I. Eremets, V.V. Struzhkin, H.-k. Mao, R.J. Hemley, Science 293 (2001) 272.
[39] D. Emin, J. Solid State Chem. 179 (2006) 2791.
[40] D. Emin, Phys. Today 40 (1987) 55.
[41] R.H. Wentorf, Science 147 (1965) 49.
[42] A.R. Oganov, V.L. Solozhenko, J. Superhard Mater. 31 (2009) 285.
[43] A.R. Oganov, J. Chen, C. Gatti, Y. Ma, Y. Ma, C.W. Glass, Z. Liu, T. Yu, O.O. Kurakevych, V.L. Solozhenko, Nature 460 (2009) 292.
[44] M.D. Segall, P.J.D. Lindan, M.J. Probert, C.J. Pickard, P.J. Hasnip, S.J. Clark, M.C. Payne, J. Phys.: Condens. Matter 14 (2002) 2717.

[45] D. Vanderbilt, Phys. Rev. B 41 (1990) 7892.
[46] D.M. Ceperley, B.J. Alder, Phys. Rev. Lett. 45 (1980) 566.
[47] J.P. Perdew, J.A. Chevary, S.H. Vosko, K.A. Jackson, M.R. Pederson, D.J. Singh, C. Fiolhais, Phys. Rev. B 46 (1992) 6671.
[48] J.P. Perdew, K. Burke, M. Ernzerhof, Phys. Rev. Lett. 77 (1996) 3865.
[49] Z.-J. Wu, E.-j. Zhao, H.-p. Xiang, X.-f. Hao, X.-j. Liu, J. Meng, Phys. Rev. B 76 (2007) 054115.
[50] A. Bouhemadou, Solid State Sci. 11 (2009) 1875.
[51] F. Gao, J. He, E. Wu, S. Liu, D. Yu, D. Li, S. Zhang, Y. Tian, Phys. Rev. Lett. 91 (2003) 015502.
[52] F. Gao, Phys. Rev. B 69 (2004) 094113.
[53] A. Bouhemadou, F. Djabi, R. Khenata, Phys. Lett. A 372 (2008) 4527.
[54] D.B. Sirdeshmukh, L. Sirdeshmukh, K.G. Subhadra, Micro-and Macro-Properties of Solids: Thermal, Mechanical and Dielectric Properties, Springer Series in Material Science, vol. 80, Springer, New York, 2006, p.315.
[55] P. Ravindran, L. Fast, P.A. Korzhavyi, B. Johnnsson, J. Wills, O. Eriksson, J. Appl. Phys. 84 (1998) 4891.
[56] O.L. Anderson, J. Phys. Chem. Solids 24 (1962) 909.
[57] S.C. Abrahams, F.S.L. Hsu, J. Chem. Phys. 63 (1975) 1162.
[58] M.J. van Setten, M.A. Uijttewaal, G.A. de Wijs, R.A. de Groot, J. Am. Chem. Soc. 129 (2007) 2458.
[59] J. Zhao, J.P. Lu, Phys. Rev. B 66 (2002) 092101.
[60] K. Shirai, H. Dekura, A. Yanase, J. Phys. Soc. Jpn. 78 (2009) 084714.
[61] K. Shirai, A. Masago, H. Katayama-Yoshida, Phys. Status Solidi (b) 244 (2007) 303.
[62] K. Shirai, A. Masago, H. Katayama-Yoshida, Phys. Status Solidi (b) 241 (2004) 3161.
[63] Y. Ma, C.T. Prewitt, G. Zou, Ho-k. Mao, J. Russell, Hemley, Phys. Rev. B 67 (2003) 174116.
[64] X. Hao, Y. Xu, Z. Wu, D. Zhou, X. Liu, X. Cao, J. Meng, Phys. Rev. B 74 (2006) 224112.
[65] Y.L. Godec, O.O. Kurakevych, P. Munsch, G. Garbarino, V.L. Solozhenko, Solid State Commun. 149 (2009) 1356.